ChemPubSoc Europe

DOI: 10.1002/ejic.201900477

EurJIC European Journal of Inorganic Chemistry

Full Paper

Double Pincer Deprotonation | *Very Important Paper* |

VIP

Sequential Double Dearomatization of the Pyrazolate-Based "Two-in-One" Pincer Ligand in a Dinuclear Rhodium(I) Complex

Alexander Gers-Barlag,[a] Pierre Goursot,[a] Ming Li,[a] Sebastian Dechert,[a] and Franc Meyer*[a]

Abstract: A binucleating pyrazolate-based ligand providing two tridentate PNN compartments is shown to form a dinuclear rhodium(I) complex [L{Rh(CO)}$_2$](PF$_6$) (**1**) that can be deprotonated at both side arm methylene groups between pyridine and phosphino donors to give K[L**{Rh(CO)}$_2$] (**3**). Sequential twofold deprotonation has been monitored by NMR and UV/Vis spectroscopy and proceeds via the neutral intermediate L*{Rh(CO)}$_2$ (**2**). X-ray crystallographic characterization of **1** and the K[2,2,2]$^+$ salt **3′** ([2,2,2] is a cryptand) evidences pyridine dearomatization upon deprotonation, and all spectroscopic and structural signatures are in good agreement with those of related mononuclear rhodium complexes based on a common PNN pincer ligand, which corroborates that pyrazolate-bridged L$^-$ is best described as a scaffold with two pincer-type subunits.

Introduction

Pincer ligands, i.e. chelating tridentate ligands that bind metal ions in a meridional configuration, have become very popular in coordination chemistry and catalysis.[1] Their successful applications often exploit metal-ligand cooperativity (MLC) which implies that both the metal ion and the ligand are involved in activating and transforming substrates, often without oxidation state changes of the metal.[2] A prominent class of pincer ligands is based on a central pyridine that is equipped with two donor substituents in the 2- and 6-positions of the heterocycle to form two five-membered chelate rings;[3,4] examples are the tridentate PNP and PNN ligands in rhodium(I) complexes **I**[5] and **II**[6] (Scheme 1). These complexes can be deprotonated at one of the methylene groups of the chelate arms to give dearomatized species (such as **III** in Scheme 1)[6,7] that are capable of heterolytically cleaving substrates X–H driven by re-aromatization.[8] Twofold pincer deprotonation is challenging but has been reported for some PNP complexes of group 10 metals,[9] and double dearomatization has recently been demonstrated for a manganese(I) complex with a {N$_2$S$_2$} donor pyridinophane ligand.[10]

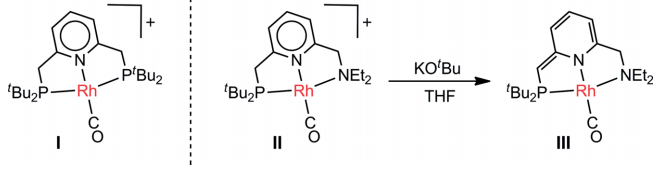

Scheme 1. Rh^{I}CO complexes of classical pincer-type PNP (**I**) and PNN (**II**) ligands and ligand dearomatization via deprotonation of **II**.[5–7]

Complementary to MLC, metal–metal cooperativity (MMC) in bi- and oligometallic complexes has emerged as a useful concept for substrate activation and catalysis, often inspired by multimetallic active sites in metalloproteins.[11] Various types of compartmental dinucleating ligands have been developed to achieve MMC,[12] and the pyrazolate heterocycle has proven valuable as a central *N*,*N*′-bridging unit in that regard.[13]

With the aim of combining both concepts and to enable MLC and MMC in a single system, we recently designed a pyrazolate-based ligand scaffold HL (see Scheme 2 below) that is comprised of two pincer-type PNN sites and can be viewed as having two fused PNN subunits akin to the PNN ligand in **II**; we coined this the "two-in-one" pincer ligand.[14] In dinuclear complexes of L$^-$ the two active coordination sites *trans* to the pyrid-

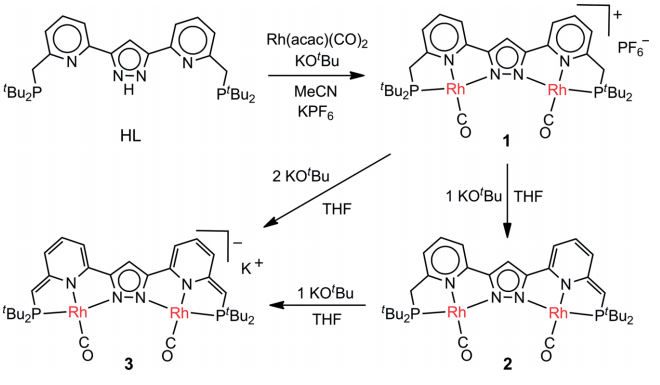

Scheme 2. Reactions studied in this work.

[a] *Institut für Anorganische Chemie, Universität Göttingen, Tammannstrasse 4, 37077 Göttingen, Germany*
E-mail: franc.meyer@chemie.uni-goettingen.de
http://www.meyer.chemie.uni-goettingen.de/index.html

Supporting information and ORCID(s) from the author(s) for this article are available on the WWW under https://doi.org/10.1002/ejic.201900477.

ine-N are directed into the bimetallic cleft, which is believed to potentially favor MMC. As such, L^- is distinct from other more flexible dinucleating ligands that feature two fused pincer-type binding sites.[15] In the initial report it was described that a diiron(II) complex of L^- shows spin state switching in solution via reversible ligand exchange processes.[14] Here we demonstrate that dinuclear complexes of L^- can undergo sequential double deprotonation and dearomatization at the two chelate arms, which is a prerequisite for achieving MLC in the way it has been successfully exploited for the mononuclear systems.[8]

Results and Discussion

Addition of two equivalents of [Rh(acac)(CO)$_2$] to a suspension containing the proligand HL, one equivalent of KO*t*Bu and KPF_6 in MeCN results in the formation of a yellow brown solution of [L{Rh(CO)}$_2$](PF$_6$) (**1**; Scheme 2). An ESI mass spectrum of the crude product gave a single dominant peak at *m*/*z* = 799.1 amu corresponding to the complex cation [L{Rh(CO)}$_2$]$^+$ (Figure S18). Crystals suitable for X-ray diffraction were grown by slow Et_2O diffusion into an acetone solution of **1**. The molecular structure of the cation is shown in Figure 1, together with selected bond lengths.

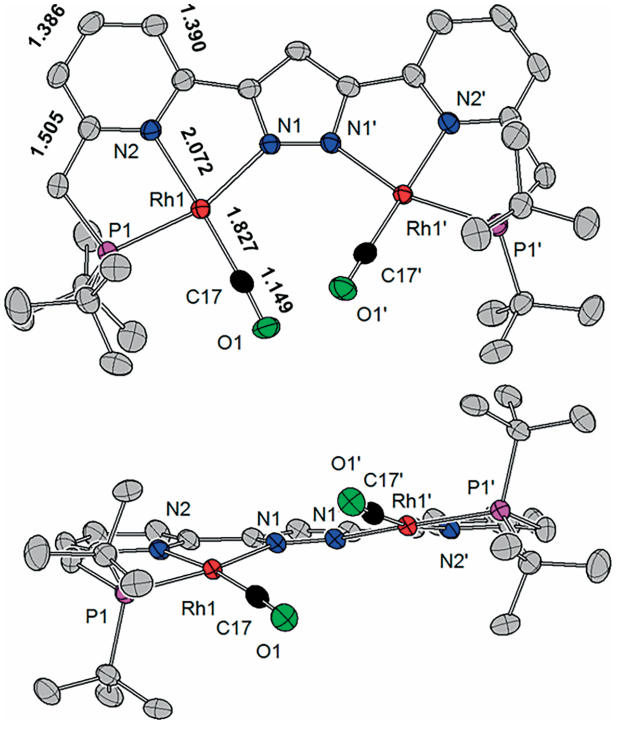

Figure 1. Top view (top) and front view (bottom) of the molecular structure of the cation of **1**. Thermal displacement ellipsoids shown at 50 % probability; hydrogen atoms, counteranion and solvent molecules omitted for clarity. Selected bond lengths are included.

As anticipated, two {Rh(CO)} units are hosted in the two PNN binding pockets of the dinucleating ligand scaffold L^- and are spanned by the bridging pyrazolate; the metal–metal distance is 4.494 Å and hence relatively long for bimetallic complexes of compartmental pyrazolate-bridging ligands.[13,16] Both rhodium(I) ions exhibit a slight distortion from square-planar coordination geometry, likely caused by the steric congestion that forces the two CO ligands, which both are directed into the bimetallic pocket, to point below and above the equatorial plane defined by the pyrazolate heterocycle (Figure 1, bottom). This results in overall C_2 symmetry of the bimetallic complex and a Rh–N–N–Rh torsion angle of 28.8(4)°. The Rh–CO {$d_{Rh\text{-}CO}$ = 1.827(3) Å} and C–O {$d_{C\text{-}O}$ = 1.149(3) Å} bond lengths are very similar to those of the mononuclear analogue [(PNP)Rh(CO)]$^+$ (**I**) {$d_{Rh\text{-}CO}$ = 1.818(5) Å}, C–O {$d_{C\text{-}O}$ = 1.144(6) Å}.[5] Complex **1** shows IR bands for the symmetric and antisymmetric CO stretching vibrations at 1964 cm^{-1} and 1978 cm^{-1}, slightly lower than the CO stretch for **I** (1982 cm^{-1})[5] but similar to that of **II** (1966 cm^{-1}).[6]

^{1}H NMR spectra of **1** in [D$_3$]MeCN show a single doublet for the CH$_2$ group at 3.81 ppm ($^2J_{PH}$ = 9.6 Hz) and a single doublet for the *t*Bu groups at 1.38 ppm ($^3J_{PH}$ = 14.5 Hz) both at 298 and 243 K, which reflects apparent C_{2v} symmetry of the bimetallic core in solution. This indicates that interconversion of the two enantiomeric forms (*P* and *M* isomers) is fast on the NMR timescale even at low temperatures. The ^{31}P{^{1}H} spectrum of **1** shows a doublet at 99.74 ppm with coupling to the nearby ^{103}Rh nucleus ($^1J_{RhP}$ = 148.1 Hz), which differs from the values for **I** [δ(^{31}P{^{1}H}) = 79.84, $^1J_{RhP}$ = 120.0 Hz][5] but is very similar to the signatures of **II** [δ(^{31}P{^{1}H}) = 98.18, $^1J_{RhP}$ = 149.4 Hz].[6] Also the ^{13}C{^{1}H} NMR resonances for the carbonyl-C atoms in **1** (δ = 194.41, $^1J_{RhC}$ = 73.8 Hz, $^2J_{CP}$ = 17.5 Hz) and **II** (δ = 193.15, $^1J_{RhC}$ = 73.7 Hz, $^2J_{CP}$ = 16.8.5 Hz)[6] are very similar. This underlines that **1** can be viewed as a bimetallic version of the classical PNN pincer-type rhodium(I) complex **II**.

To probe the deprotonation of **1** akin to the dearomatization of **II** shown in Scheme 1, a suspension of microcrystalline material of **1** in THF was titrated with KO*t*Bu. Upon addition of one equivalent of KO*t*Bu an immediate color change from yellow to green is observed, and addition of a second equivalent of KO*t*Bu then leads to further color change to deep purple. These observations are interpreted in terms of a stepwise deprotonation of the ligand scaffold L^- to give complexes [L*{Rh(CO)}$_2$] (**2**) and K[L**{Rh(CO)}$_2$] (**3**) as shown in Scheme 2. However, because of differences in solubility (**2** and **3** are soluble in THF whereas **1** is insoluble in THF but soluble in MeCN), only the second titration step could be monitored in situ by NMR and UV/Vis spectroscopy (see Figure 2). The latter shows three isosbestic points and the gradual disappearance of the band at 391 nm characteristic of **2** and the increase in absorption at 350 and 560 nm indicative of formation of **3**. The low-energy absorptions are tentatively assigned to ligand-to-metal charge transfer (LMCT) transitions involving the dearomatized pyridine groups. Only singly deprotonated **2** (and not a mixture containing **1**, **2** and doubly deprotonated **3**) is observed after treating **1** with one equivalent of KO*t*Bu, which indicates that the pK_a for the second deprotonation is higher than for the first.

Figure 3 shows a comparison of relevant parts of the ^{1}H and ^{31}P{^{1}H} NMR spectra of **1** in [D$_3$]MeCN (bottom) and of **2** (middle) and **3** (top) in [D$_8$]THF. In **3** both the ^{31}P as well as the ^{1}H NMR resonances are shifted substantially upfield compared to **1**. ^{1}H NMR signals in the range 5.3 – 6.3 ppm (vs. 7.2–8.0 in **1**) provide clear evidence of dearomatization of the pyridine groups in **3**. In analogy to other deprotonated 2-(di-*tert*-butyl-

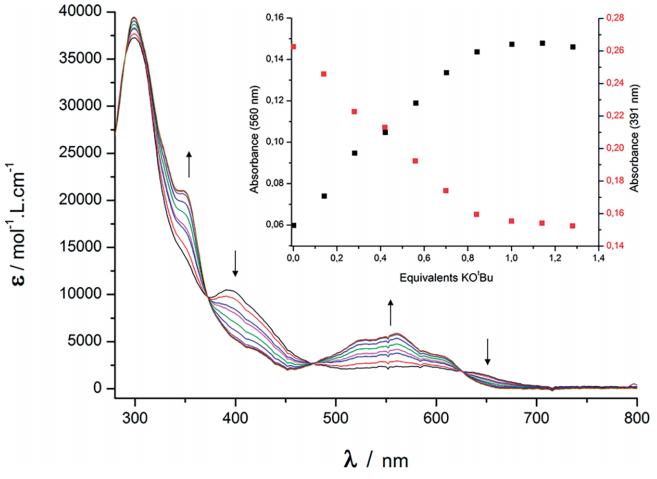

Figure 2. Monitoring the second deprotonation that converts **2** into **3** in THF solution; the inset shows the evolution of the bands at 560 and 391 nm upon titration with KO*t*Bu (aliquots of 0.14 equivalents).

phosphinomethyl)pyridine derivatives,[17] the proton at the 4-position of the dearomatized pyridine gives rise to a doublet of doublets of doublets, which includes coupling with the phosphorus atom in the deprotonated chelate arm ($^5J_{HP}$ = 2.2 Hz). The ^{31}P NMR resonance shifts upfield from 99.74 ppm in **1** to 87.83 ppm in **3**, but $^1J_{RhP}$ does not change much (155 Hz vs. 148 Hz). The upfield shift upon dearomatization of $\Delta\delta(^{31}P)$ = 11.9 ppm is even more pronounced than in the case of **II**→**III** [$\Delta\delta(^{31}P)$ = 7.3 ppm].[6] Similar to the situation in **1**, twice deprotonated **3** shows only a single doublet for the *t*Bu groups (at 1.37 ppm, $^3J_{PH}$ = 13.0 Hz), indicative of apparent C_{2v} symmetry on the NMR timescale even at low temperatures (208 K).

Singly deprotonated **2** shows two sets of resonances in both its ^{1}H and ^{31}P{^{1}H} NMR spectra [e.g., $\delta(^{31}P\{^1H\})$ = 97.78 and 88.58 ppm] reflecting the presence of each one protonated and one deprotonated (viz. dearomatized) ligand half. Interestingly, however, the separation of the two signal sets is less than expected from the signal positions of the fully protonated and deprotonated congeners **1** and **3** (see Figure 3), which suggests some interaction between the two subunits in **2**. The singlet for the central backbone pyrazolate-H[4] exhibits an almost linear shift from 7.27 ppm in **1** to 6.67 ppm in **2** and 6.17 ppm in **3**.

Addition of a stoichiometric amount of [2,2,2] cryptand (4,7,13,21,24-hexaoxa-1,10-diazabicyclo[8.8.8]hexacosane) to the solution containing **3** allowed to isolate the anionic dirhodium(I) complex as the K[2,2,2]$^+$ salt **3′**, so that crystals suitable for X-ray diffraction could be obtained. The molecular structure of the cation is presented in Figure 4.

Inspection of the atom distances in the chelate arms shows alternating bond lengths and more localized double bonds, which confirms the dearomatization of the pyridine rings. Most pronounced is the change for the exocyclic C–C bond which shortens from 1.505 Å in **1** to 1.362/1.381 Å in **3′**. Overall this leads to rigidification and flattening of the bimetallic scaffold, and thus to a decreased Rh–N–N–Rh torsion angle of 15.3(13)°; as a consequence the Rh···Rh distance in **3′** [4.3861(12) Å] is shorter than in **1** [4.4944(7) Å]. Furthermore, in comparison with **1** the Rh–N^{py} and Rh–C^{CO} bonds are slightly shorter while the C–O bond is somewhat longer (Table S2). This reflects the higher donor strength of the anionic dearomatized pyridine and increased Rh→CO π-backbonding in **3′**. The trends are mirrored in the IR spectra of solid material of **1** and **3′** (shown in Figure 5) where the CO stretching vibrations shift from 1978 and 1964 cm^{-1} in **1** to 1951 and 1923 cm^{-1} in **3′**. This is in line with the trend reported for the corresponding mononuclear Rh–PNN complex for which the CO stretch shifts from 1966 cm^{-1} in **II** to 1939 cm^{-1} in **III**.[6] The larger separation of the two bands in **3′** ($\Delta\nu_{C-O}$ = 28 cm^{-1}) compared to **1** ($\Delta\nu_{C-O}$ = 14 cm^{-1}) suggests that vibronic coupling is enhanced in the

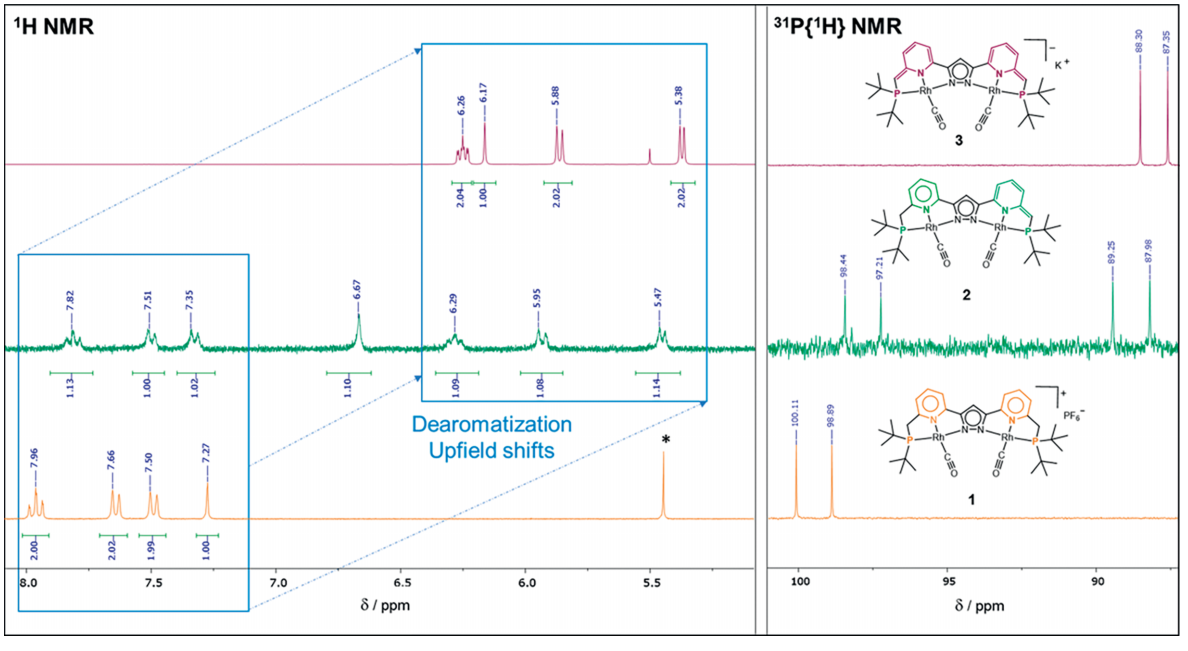

Figure 3. ^{1}H NMR spectra at 298 K of **3** (top, [D$_8$]THF, 500 MHz), **2** (middle, [D$_8$]THF, 400 MHz) and **1** (bottom, [D$_3$]MeCN, 400 MHz).

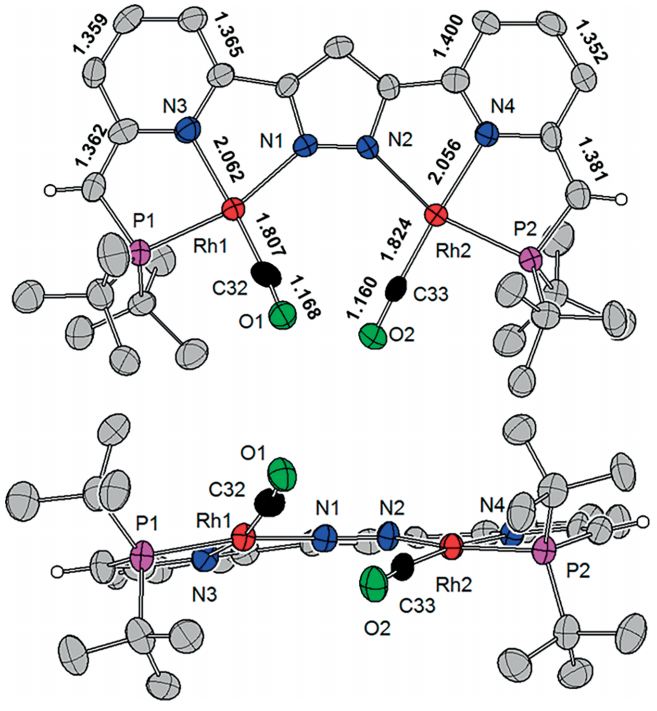

Figure 4. Top view (top) and front view (bottom) of the molecular structure of the anion of **3′**. Thermal displacement ellipsoids shown at 50 % probability; most hydrogen atoms, the cation K[2,2,2]$^+$ and solvent molecules omitted for clarity. Selected bond lengths are included.

rigidified and flattened framework. The IR bands at 1606 and 1564 cm^{-1} for **1** are assigned to the coordinated pyridine ring, and these appear at 1606 and 1537 cm^{-1} after dearomatization; shifts of IR bands from 1606/1565 cm^{-1} to 1634/1540 cm^{-1} upon dearomatization have been reported for related mononuclear Ni–PNP complexes.[18]

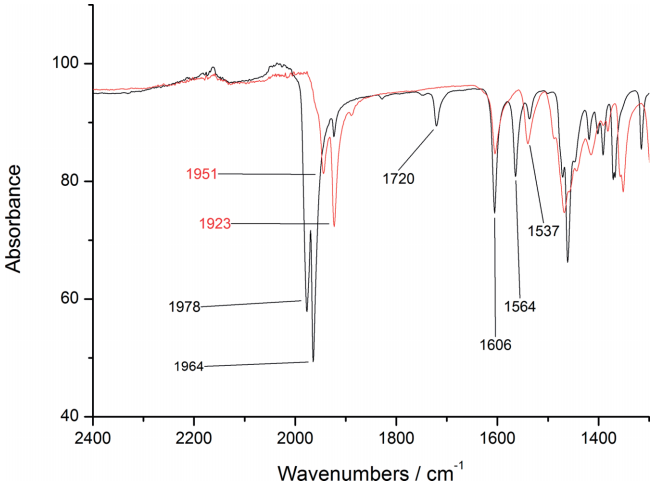

Figure 5. ATR-IR spectra of solid samples of **1** (black line) and **3′** (red line). The band at 1720 cm-1 originates from acetone contained in the crystalline material of **1**.

Treatment of a solution of **3** in THF with H_2O or MeOH cleanly re-forms **1** which precipitates as a yellow solid from the reaction mixtures, demonstrating reversibility of the deprotonation and facile re-aromatization. No reaction of complex **3** with H_2 was observed even at pressures up to 10 bar or at low temperatures, which indicates that the strongly bound CO ligands need to be replaced by more labile ligands to achieve interesting reactivity. Studies in that direction are in progress.

Conclusions

When we first reported the pyrazolate-based dinucleating scaffold [L]$^-$ we described it as having two fused pincer-type PNN compartments and thus dubbed it "two-in-one" pincer ligand.[14] Following the initial report of its diiron(II) complex,[14] the present study now introduces a first dinuclear 4d metal complex of [L]$^-$ and demonstrates its close similarity with related mononuclear PNN pincer systems, thus validating the view that [L]$^-$ provides two closely spaced pincer sites. Specifically, it is shown that the dirhodium(I) complex [L{Rh(CO)}$_2$](PF$_6$) (**1**) can be sequentially deprotonated at the two side arm methylene groups along with twofold pyridine dearomatization, and all spectroscopic and structural signatures of **1** and its twice deprotonated congener K[L**{Rh(CO)}$_2$] (**3**) are in good agreement with those of the related mononuclear [(PNN)Rh(CO)]$^{+/0}$ complexes. This now promises that doubly dearomatized complexes akin to **3** may enable new substrate activation trajectories that involve the heterolytic cleavage of two X–H functions driven by pyridine re-aromatization, potentially combining MLC and MMC chemistries.

Experimental Section

General Considerations and Methods: All experiments were carried out under an atmosphere of purified dinitrogen in MBraun gloveboxes (Labmaster and Unilab) or using standard Schlenk techniques under an atmosphere of purified argon. All solvents were used in reagent grade or better. Non-deuterated solvents were heated to reflux over sodium/benzophenone ketyl, then distilled under an argon atmosphere and degassed with argon prior use. [D$_6$]Acetone was refluxed over B_2O_3 and distilled under an argon atmosphere. Other deuterated solvents were dried with activated molecular sieves (3 Å). All deuterated solvents were degassed via freeze-pump-thaw cycles. Commercially available reagents were used as received. The proligand HL was prepared according to a literature procedure.[14]

NMR spectra were recorded on a Bruker Avance III HD 500 (^{1}H 500 MHz, ^{13}C 126 MHz, ^{31}P 202 MHz), a Bruker Avance III HD 400, a Bruker Avance III 400 (both: ^{1}H 400 MHz, ^{13}C 100 MHz, ^{31}P 162 MHz) and a Bruker Avance III 300 (^{1}H 300 MHz, ^{13}C 75 MHz, ^{31}P 121 MHz). If not mentioned otherwise, all spectra were measured at 298 K. ^{1}H NMR and ^{13}C{^{1}H} NMR chemical shifts are reported in parts per million downfield from tetramethylsilane. ^{1}H NMR chemical shifts were referenced to the residual hydrogen signals of the deuterated solvents (3.58 and 1.72 ppm for [D$_8$]THF; 1.94 ppm for [D$_3$]MeCN), and the ^{13}C NMR chemical shifts were referenced to the ^{13}C signals of the deuterated solvents (67.21 and 25.31 ppm for [D$_8$]THF; 118.26 and 1.32 ppm for [D$_3$]MeCN). Abbreviations used in the description of NMR data are as follows: s, singlet; d, doublet; t, triplet; hept, heptet; m, multiplet; py, pyridine; py$_{dearom}$, dearomatized pyridine; pz, pyrazole. IR spectra were measured with an Agilent Technologies Cary 630 FTIR. Elemental analyses were performed by the analytical laboratory of the Institute of Inorganic

Chemistry at Georg-August University Göttingen using an Elementar Vario EL III instrument. ESI mass spectra were recorded with a Bruker HCT Ultra connected to an argon glovebox, or with a Bruker maXis ESI-QTOF. X-ray crystallographic data were collected on a STOE IPDS II diffractometer (graphite monochromated Mo-Kα radiation, λ = 0.71073 Å) by use of □ scans at –140 °C; details of the data collection and structure analyses can be found in the Supporting Information. CCDC 1911607 (for **1**), and 1911608 (for **3′**) contain the supplementary crystallographic data for this paper. These data can be obtained free of charge from The Cambridge Crystallographic Data Centre.

[L{Rh(CO)}$_2$](PF$_6$) (1): To a suspension of HL (25.0 mg, 46.4 µmol, 1.0 equiv.), KO*t*Bu (5.20 mg, 46.4 µmol, 1.0 equiv.) and KPF_6 (10.2 mg, 55.7 µmol, 1.2 equiv.) in MeCN (4 mL) was added solid [Rh(acac)(CO)$_2$] (23.9 mg, 92.8 µmol, 2.0 equiv.). The reaction mixture was stirred at ambient temperature for 23 h, volatiles were then removed in vacuo and the residue was extracted with CH_2Cl_2 (2 × 3 mL) to give the crude product. Crystals suitable for X-ray diffraction were obtained by diffusion of Et_2O into a concentrated acetone solution of **1** (yield of crystalline material: 28 %). ^{1}H NMR (400 MHz, CD_3CN) δ = 7.96 (td, $J_{H\text{-}H}$ = 7.9, 1.1 Hz, 2H, py H4), 7.64 (d, $J_{H\text{-}H}$ = 7.8 Hz, 2H, py H3), 7.49 (d, $J_{H\text{-}H}$ = 7.9 Hz, 2H, py H5), 7.27 (s, 1H, pz), 3.81 (d, $J_{P\text{-}H}$ = 9.6 Hz, 4H, CH_2), 1.38 (d, $J_{P\text{-}H}$ = 14.5 Hz, 36H, C(*C*H$_3$)$_3$). ^{13}C NMR (126 MHz, CD_3CN) δ = 194.43 (dd, $J_{Rh\text{-}C}$ = 73.8 Hz, $J_{P\text{-}C}$ = 17.5 Hz, CO), 163.91 (dd, $J_{Rh\text{-}C}$ = 4.8 Hz, $J_{P\text{-}C}$ = 3.2 Hz, py C6), 155.90 (dt, $J_{P\text{-}C}$ = 3.5, 1.7 Hz, pz C3/C5), 153.48 (s, py C2), 142.06 (d, $J_{P\text{-}C}$ = 0.7 Hz, py C4), 122.13 (dd, $J_{Rh\text{-}C}$ = 10.4 Hz, $J_{P\text{-}C}$ = 1.0 Hz, py C5), 118.70 (d, $J_{P\text{-}C}$ = 0.6 Hz, py C3), 103.48 (s, pz C4), 36.88 (d, $J_{P\text{-}C}$ = 22.4 Hz, *C*(CH$_3$)$_3$), 36.73 (dd, $J_{Rh\text{-}C}$ = 21.7 Hz, $J_{P\text{-}C}$ = 2.0 Hz, CH_2), 29.33 (dd, $J_{Rh\text{-}C}$ = 4.4 Hz, $J_{P\text{-}C}$ = 0.7 Hz, C(*C*H$_3$)$_3$). ^{31}P NMR (162 MHz, CD_3CN) δ = 99.74(d, $J_{Rh\text{-}P}$ = 148.1 Hz), –144.25 (hept, $J_{F\text{-}P}$ = 706.3 Hz). ATR-IR (solid): ν_{CO} = 1978, 1964 cm^{-1}. ESI-MS (MeCN): *m/z* (%) = 799.125 (100, [(Rh(CO))$_2$L$^{t\text{Bu}}$]$^+$). Anal. Calcd. for complex **1**·2H$_2$O ($C_{33}H_{51}F_6N_4O_4P_3Rh_2$): C 40.40, H 5.24, N 5.71; found C 40.44, H 5.02, N 5.40; although the sample was dried at 50 °C under vacuum for several hours the remaining water could not be removed.

[L*{Rh(CO)}$_2$] (2): A solution of KO*t*Bu (1.8 mg, 15.9 µmol, 1.0 equiv.) in THF (2 mL) was added to solid **1** (15.0 mg, 15.9 µmol, 1.0 equiv.). The suspension turned green within 5 min and was stirred at ambient temperature for 2 h. The reaction mixture was filtered through a glass fibre filter and the volatiles were removed in vacuo to obtain 9 mg (71 %) of **2** as a green solid. ^{1}H-NMR (400 MHz, [D$_8$]THF) δ = 7.82 (t, *J* = 7.6 Hz, 1H, py$_{arom}$ 4-H), 7.50 (d, *J* = 7.8 Hz, 1H, py$_{arom}$ 3-H), 7.33 (d, *J* = 7.0 Hz, 1H, py$_{arom}$ 5-H), 6.67 (s, 1H, pz 4-H), 6.29 (t, *J* = 7.1 Hz, 1H, py$_{dearom}$ 4-H), 5.94 (d, *J* = 8.7 Hz, 1H, py$_{dearom}$ 3-H), 5.45 (d, *J* = 6.8 Hz, 1H, py$_{dearom}$ 5-H), 3.78 (d, *J* = 10.3 Hz, 2H, CH_2), 3.11 (d, *J* = 3.6 Hz, 1H, CH), 1.42 (d, *J* = 9.9 Hz, 18H, C(CH$_3$)$_3$), 1.37 (d, *J* = 9.0 Hz, 18H, C(CH$_3$)$_3$). ^{31}P-NMR (162 MHz, [D$_8$]THF) δ = 97.82 (d, *J* = 149.2 Hz, P$_{arom}$), 88.62 (d, *J* = 154.4 Hz, P$_{dearom}$), –144.26 (hept, $J_{F\text{-}P}$ = 708.5 Hz). ATR-IR (solid): ν_{CO} = 1990, 1940 cm^{-1}.

K[L{Rh(CO)}$_2$] (3):** A solution of KO*t*Bu (3.6 mg, 31.8 µmol, 2.0 equiv.) in THF (2 mL) was added to solid **1** (15.0 mg, 15.9 µmol, 1.0 equiv.). The suspension turned deep purple within 5 min and was stirred at ambient temperature for 2 h. The reaction mixture was filtered through a glass fibre filter and the volatiles were removed in vacuo to obtain 11 mg (83 %) of crude **3** as a purple solid. ^{1}H-NMR (400 MHz, [D$_8$]THF) δ = 6.26 (ddd, *J* = 8.8, 6.6, 2.2 Hz, 2H, py$_{dearom}$ 4-H), 6.17 (s, 1H, pz 4-H), 5.87 (d, *J* = 8.8 Hz, 2H, py$_{dearom}$ 3-H), 5.38 (dd, *J* = 6.6, 1.1 Hz, 2H, py$_{dearom}$ 5-H), 3.06 (d, *J* = 2.3 Hz, 2H, CH), 1.36 (d, *J* = 13.1 Hz, 36H, C(CH$_3$)$_3$). ^{13}C NMR (126 MHz, [D$_8$]THF) δ = 197.7 (dd, $J_{Rh\text{-}C}$ = 70.3 Hz, $J_{P\text{-}C}$ = 17.1 Hz, CO), 169.8 (dd, $J_{Rh\text{-}C}$ = 18.5, $J_{P\text{-}C}$ = 3.7 Hz, py C-6), 157.7 (d, $J_{P\text{-}C}$ = 3.0 Hz, pz C-3/C-5), 152.7 (s, py C-2), 133.2 (s, py$_{dearom}$ C-4), 113.1 (d, *J* = 18.7 Hz, py$_{dearom}$ C-3), 97.2 (s, pz C-4), 95.5 (s, py$_{dearom}$ C-5), 62.0 (d, *J* = 56.0 Hz, CH), 36.9 (dd, *J* = 26.2, 2.0 Hz, *C*(CH$_3$)$_3$), 30.4 (d, *J* = 5.2 Hz, C(*C*H$_3$)$_3$). ^{31}P-NMR (162 MHz, [D$_8$]THF) δ = 87.83 (d, *J* = 152.7 Hz). ATR-IR (solid): ν_{CO} = 1964, 1940 cm^{-1}.

[K(C$_{18}$H$_{36}$N$_2$O$_6$)][L{Rh(CO)}$_2$] (3′):** A solution of KO*t*Bu (9.5 mg, 84.7 µmol, 2.0 equiv.) in THF (2 mL) was added to solid **1** (40.0 mg, 42.4 µmol, 1.0 equiv.). Solid cryptand [2,2,2] (16.0 mg, 42.5 µmol, 1.0 equiv.) was added to the deep purple solution. Slow pentane diffusion into the mixture at –35 °C yielded dark brown needles. The crystals were isolated and carefully dried to yield 42 mg (82 %) of **3**. ^{1}H-NMR (500 MHz, [D$_8$]THF) δ = 6.24 (ddd, *J* = 8.8, 6.6, 2.1 Hz, 2H, py$_{dearom}$ 4-H), 6.13 (s, 1H, pz 4-H), 5.84 (d, *J* = 8.8 Hz, 2H, py$_{dearom}$ 3-H), 5.36 (dd, *J* = 6.6, 1.1 Hz, 2H, py$_{dearom}$ 5-H), 3.56 (s, 12H, CH_2 cryptand), 3.50 (t, *J* = 4.6 Hz, 12H, CH_2 cryptand), 3.04 (d, *J* = 2.3 Hz, 2H, CH), 2.50 (t, *J* = 4.6 Hz, 12H, CH_2 cryptand), 1.37 (d, *J* = 13.0 Hz, 36H, C(CH$_3$)$_3$). ^{13}C NMR (126 MHz, [D$_8$]THF) δ = 197.6 (dd, $J_{Rh\text{-}C}$ = 70.7 Hz, $J_{P\text{-}C}$ = 17.3 Hz, CO), 169.6 (dd, $J_{Rh\text{-}C}$ = 18.7, $J_{P\text{-}C}$ = 3.8 Hz, py C-6), 157.0 (d, $J_{P\text{-}C}$ = 3.2 Hz, pz C-3/C-5), 152.9 (s, py C-2), 133.0 (s, py$_{dearom}$ C-4), 112.4 (d, *J* = 18.5 Hz, py$_{dearom}$ C-3), 96.9 (s, pz C-4), 95.0 (s, py$_{dearom}$ C-5), 71.5 (s, CH_2 cryptand), 68.5 (s, CH_2 cryptand), 68.2 (s, CH_2 cryptand), 67.9 (s, CH_2 cryptand), 61.6 (d, *J* = 55.7 Hz, CH), 54.8 (s, CH_2 cryptand), 36.7 (dd, *J* = 26.0, 2.0 Hz, *C*(CH$_3$)$_3$), 30.3 (d, *J* = 5.2 Hz, C(*C*H$_3$)$_3$). ^{31}P-NMR (203 MHz, [D$_8$]THF) δ = 87.83 (d, *J* = 155.0 Hz). ATR-IR (solid): ν_{CO} = 1951, 1923 cm^{-1}. Anal. Calcd. for complex **3′** ($C_{51}H_{81}N_6O_8P_2KRh_2$): C 50.48, H 6.73, N 6.93; found C 50.03, H 6.77, N 6.52.

Acknowledgments

Support of this work by the Georg-August-University Göttingen is gratefully acknowledged.

Keywords: Pincer ligands · Rhodium · Bimetallic complexes · Pyrazolate ligands · Structure elucidation · Dearomatization

[1] a) G. van Koten, *J. Organomet. Chem.* **2013**, *730*, 156–164; b) P. A. Chase, R. A. Gossage, G. van Koten, *The Privileged Pincer-Metal Platform: Coordination Chemistry & Applications*, *Vol. 54*, (Eds.: G van Koten, R. A. Gossage), *Springer*, Switzerland, **2016**, pp. 1–15; c) M. A. W. Lawrence, K. A. Green, P. N. Nelson, S. C. Lorraine, *Polyhedron* **2018**, *143*, 11–27; d) A. Mukherjee, D. Milstein, *ACS Catal.* **2018**, *8*, 11435–11469; e) L. Alig, M. Fritz, S. Schneider, *Chem. Rev.* **2019**, *119*, 2681–2751.

[2] a) H. Grützmacher, *Angew. Chem. Int. Ed.* **2008**, *47*, 1814–1818; *Angew. Chem.* **2008**, *120*, 1838; b) D. Gelman, S. Musa, *ACS Catal.* **2012**, *2*, 2456–2466; c) J. R. Khusnutdinova, D. Milstein, *Angew. Chem. Int. Ed.* **2015**, *54*, 12236–12273; *Angew. Chem.* **2015**, *127*, 12406; d) P. A. Dub, J. C. Gordon, *ACS Catal.* **2017**, *7*, 6635–6655; e) M. D. Wodrich, X. Hu, *Nat. Rev. Chem.* **2017**, *2*, 99.

[3] D. Milstein, *Top. Catal.* **2010**, *53*, 915–923.

[4] D. Hermann, M. Gandelman, H. Rozenberg, L. J. W. Shimon, D. Milstein, *Organometallics* **2002**, *21*, 812–818.

[5] M. Feller, E. Ben-Ari, T. Gupta, L. J. W. Shimon, G. Leitus, Y. Diskin-Posner, L. Weiner, D. Milstein, *Inorg. Chem.* **2007**, *46*, 10479–10490.

[6] M. Feller, Y. Diskin-Posner, L. J. W. Shimon, E. Ben-Ari, D. Milstein, *Organometallics* **2012**, *31*, 4083–4101.

[7] L. Schwartsburd, M. A. Iron, L. Konstantinovski, E. Ben-Ari, D. Milstein, *Organometallics* **2011**, *30*, 2721–2729.

[8] a) C. Gunanathan, D. Milstein, *Acc. Chem. Res.* **2011**, *44*, 588–602; b) D. Milstein, *Phil. Trans. R. Soc. A* **2015**, *373*, 1–10; c) H. Li, M. B. Hall, *ACS Catal.* **2015**, *5*, 1895–1913.

[9] a) M. Feller, E. Ben-Ari, M. A. Iron, Y. Diskin-Posner, G. Leitus, L. J. W. Shimon, L. Konstantinovski, D. Milstein, *Inorg. Chem.* **2010**, *49*, 1615–1625; b) M. Vogt, O. Rivada-Wheelaghan, M. A. Iron, G. Leitus, Y. Diskin-Posner, L. J. W. Shimon, Y. Ben-David, D. Milstein, *Organometallics* **2013**, *32*, 300–308.

[10] A. Sarbajna, P. H. Patil, M. H. Dinh, O. Gladkovskaya, R. R. Fayzullin, S. Lapointe, E. Khaskina, J. R. Khusnutdinova, *Chem. Commun.* **2019**, *55*, 3282–3285.

[11] a) D. G. McCollum, B. Bosnich, *Inorg. Chim. Acta* **1998**, *270*, 13–19; b) J. I. van der Vlugt, *Eur. J. Inorg. Chem.* **2012**, 363–375; c) J. Park, S. Hong, *Chem. Soc. Rev.* **2012**, *41*, 6931–6943; d) M. Ainooson, F. Meyer in *Comprehensive Inorg. Chemistry II, Vol. 8* (Eds.: J. Reedijk, K. Poeppelmeier), Elsevier, Oxford, **2013**, pp. 433–458.

[12] A. L. Gavrilova, B. Bosnich, *Chem. Rev.* **2004**, *104*, 349–383.

[13] a) J. Klingele, S. Dechert, F. Meyer, *Coord. Chem. Rev.* **2009**, *253*, 2698–2741; K. E. Dalle, F. Meyer, *Eur. J. Inorg. Chem.* **2015**, 3391–3405.

[14] S. Samanta, S. Demesko, S. Dechert, F. Meyer, *Angew. Chem. Int. Ed.* **2015**, *54*, 583–587; *Angew. Chem.* **2015**, *127*, 593.

[15] D. Wang, S. V. Lindeman, A. T. Fiedler, *Inorg. Chem.* **2015**, *54*, 8744–8754.

[16] a) T. G. Schenck, C. R. C. Milne, J. F. Sawyer, B. Bosnich, *Inorg. Chem.* **1985**, *24*, 2338–2344; b) A. Gondoh, T. Koike, M. Akita, *Inorg. Chim. Acta* **2011**, *374*, 489–498.

[17] T. Simler, L. Karmazin, C. Bailly, P. Braunstein, A. A. Danopoulos, *Organometallics* **2016**, *35*, 903-912.

[18] J. I. van der Vlugt, M. Lutz, E. A. Pidko, D. Vogt, A. L. Spek, *Dalton Trans.* **2009**, 1016–1023.

Received: May 1, 2019